Evaluation of Thermodynamic Properties of Solids by Quasiharmonic Lattice Dynamics

N.L. Allan[1], G.D. Barrera[2], T.H.K. Barron[1,3] and M.B. Taylor[1]

[1] School of Chemistry, University of Bristol, Cantock's Close, Bristol BS8 1TS, U.K.

[2] Departamento de Química, Universidad Nacional de la Patagonia SJB, Ciudad Universitaria, (9000) Comodoro Rivadavia , Argentina.

[3] To whom correspondence should be addressed.

ABSTRACT

Quasiharmonic Lattice Dynamics is a simulation technique complementary to Monte Carlo and Molecular Dynamics. Quantum effects are readily taken into account, and high precision does not normally require long runs. Vibrational stability is a sensitive test of interatomic potentials, and details of the vibrational motion reveal mechanisms for phase transitions or for thermal expansion. The major computational task is usually to find the equilibrium geometry at given *T*, *P*; this done, calculating free energy, heat capacity, thermal expansion, etc., is rapid and accurate. For three dimensional ionic crystals and slabs, our code SHELL calculates *analytically* first derivatives of the free energy with respect to all strains, internal as well as external; this gives a full minimisation of the free energy so efficient that *large unit cells* can be used, allowing applications to defects and disordered systems.

Various applications are discussed: MgF_2 including the rutile/fluorite transition; negative thermal expansion in ZrW_2O_8; anisotropic expansion of polyethylene at very low temperatures; surface free energies for MgO; defect energies and volumes in MgO; and a new method for obtaining free energies and phase diagrams of disordered solids and solid solutions, applied to MnO/MgO and CaO/MgO.

KEY WORDS: defects; free energy minimisation; lattice dynamics; low temperatures; solid solutions; thermal expansion.

1. INTRODUCTION

Quasiharmonic lattice dynamics (QLD) is a relatively inexpensive technique, which avoids the kinetic barriers and critical slowing-down effects suffered by Monte Carlo (MC) and molecular dynamics (MD), and has the advantage that free energies and derived properties such as entropy and heat capacity can be calculated directly to high precision. QLD also gives a sensitive test for interatomic potentials in that imaginary phonon frequencies may indicate at once that a trial potential is invalid. The main disadvantage is that QLD is valid only when vibrational amplitudes are fairly small, and so other techniques must be used at high temperatures as melting is approached. We first outline the technique, as applied by our recent code SHELL [1], and then present the set of illustrative examples listed in the Abstract.

2. THEORETICAL METHODS

Our new code SHELL [1] uses both lattice statics and QLD, and is designed for the efficient study of solids and slabs with periodic structures and *many* internal strains. In its present form two- and three-body potentials represent short-range forces. Ionic and polarizability effects are taken into account by using the well-known shell model, in which each ion consists of a massive ‘core’ and massless ‘shell’; both core and shell are charged, and so their relative displacement produces an electric dipole.

For structure optimisation, we minimise the free energy using its strain derivatives. Most previous work has used the zero static internal stress approximation (ZSISA), or minor variations thereof, in which only external coordinates (dimensions of the unit cell) are relaxed using fully dynamic free energy derivatives, while internal coordinates (positions of the ions in the unit cell) are relaxed using static energy derivatives. The static energy derivatives are easy to calculate analytically and the small

number of external free energy derivatives are obtained numerically. ZSISA gives optimised external coordinates correctly to first order [2], but to get correct internal coordinates requires a full minimisation of the free energy with respect to all coordinates; and even for moderately sized unit cells to do this by numerical differentiation is normally prohibitively expensive. SHELL therefore adopts a method suggested for complex ionic crystals by Kantorovich [3], and calculates the full set of free energy first derivatives analytically; this makes possible a valid treatment of the atomic positions within the unit cell.

For optimisation at an applied pressure P_{ext} we minimize the 'availabilty' [4] $\tilde{G} = F + P_{\text{ext}}V$ with respect to all strains. In QLD the Helmholtz free energy, F, at temperature T is the sum of static and vibrational contributions:

$$F(\mathscr{E}, T) = \Phi_{\text{stat}}(\mathscr{E}) + F_{\text{vib}}(\mathscr{E}, T)$$

where $\mathscr{E}$ denotes the full set of strain variables, comprising both external (η_λ) and internal (ε_k) strains. Φ_{stat} is thus the potential energy of the static lattice in a given state of strain $\mathscr{E}$. Traditional static lattice simulations evaluate only Φ_{stat} and its strain derivatives.

F_{vib} is the sum of harmonic vibrational contributions from all the normal modes of vibration, and for a periodic structure is given by:

$$F_{\text{vib}} = \sum_{\mathbf{q},j} \left\{ \tfrac{1}{2} h\nu_j(\mathbf{q}) + k_B T \ln\left[1 - \exp\left(-h\nu_j(\mathbf{q}) / k_B T\right)\right] \right\}$$

in which the first term is the zero-point energy. The frequencies $\nu_j(\mathbf{q})$ of modes with wavevector $\mathbf{q}$ are obtained by diagonalising the dynamical matrix $D(\mathbf{q})$ [5] which is a function of the strain $\mathscr{E}$. The strain derivatives are given by

$$\left(\frac{\partial F_{\mathrm{vib}}}{\partial \mathscr{E}_A}\right)_{\mathscr{E}',T} = \sum_{\mathbf{q},j}\left\{\frac{h}{2\nu_j(\mathbf{q})}\left(\frac{1}{2}+\frac{1}{\exp\left(h\nu_j(\mathbf{q})/k_BT\right)-1}\right)\left(\frac{\partial \nu_j^2(\mathbf{q})}{\partial \mathscr{E}_A}\right)_{\mathscr{E}'}\right\}$$

where $\mathscr{E}'$ denotes that all the $\mathscr{E}$ are kept constant except for the differentiation variable $\mathscr{E}_A$. SHELL uses first-order perturbation theory to derive $(\partial\nu_j^2(\mathbf{q})/\partial\mathscr{E}_A)_{\mathscr{E}'}$ from analytic expressions for $(\partial D/\partial\mathscr{E}_A)_{\mathscr{E}'}$. Details and full expressions are given in refs. 6, 7, and 8. A variable metric method [9] is used to minimise $F+P_{\mathrm{ext}}V$ with respect to the $\mathscr{E}_A$. The static energy Hessian, $(\partial^2\Phi_{\mathrm{stat}}/\partial\mathscr{E}_A\partial\mathscr{E}_B)$ is used as an approximation to $(\partial^2F/\partial\mathscr{E}_A\partial\mathscr{E}_B)$ in the first step; in subsequent iterations the $(\partial F/\partial\mathscr{E}_A)$ are calculated in the new configuration and the inverse Hessian updated.

The reliability of QLD at high temperatures can be investigated by comparison with classical MC or MD simulations. For ionic solids we have found that QLD is usually valid up to about one-half to two-thirds of the melting point.

3. APPLICATIONS

3.1 MgF_2

Our simplest example is the rutile phase of MgF_2, which has a small unit cell with only one internal degree of freedom. The potentials are derived from a calculated Hartree-Fock (HF) potential energy hypersurface [10]. We have carried out not only QLD, but also MD and MC simulations for comparison. The last two used a simulation cell containing 192 Mg and 384 F ions arranged initially in a box of sides 4x4.52 Å, 4x4.52 Å and 6x3.09 Å. In the MC simulations, the thermodynamic data were collected over 10^7 steps after a 10^7 step equilibration.

HF theory generally overestimates lattice parameters, and for MgF_2 the HF lattice parameters *a* and *c* are slightly larger than experiment [11]. For the new potential

obtained by fitting to HF energies, *a* is too small by about 0.3% and *c* too large by about 4% (Fig. 1). However, the variation with *T* of *a* and *c* is close to experiment. *Below* the Debye temperature (Θ_D) the MC values for *a* and *c* are slightly lower than the QLD values, because only QLD takes account of quantum effects (largely zero-point vibration) which expand the lattice by a small amount. The MC and MD results are in good agreement. Around Θ_D the QLD results are in good agreement with MC and MD, but for $T \geq 1300$ K they diverge, a characteristic indication that the quasiharmonic approximation is starting to fail.

Simulations are a valuable means of examining widely used quantities for which data are sparse. For example, one key quantity in geophysics is the isothermal Anderson-Grüneisen function, δ_T, and its variation with pressure,

$$\delta_T = -(\partial \ln B_T / \partial \ln V)_P = -(\partial \ln \beta / \partial \ln V)_T$$

where β is the volumetric thermal expansion coefficient ($= (\partial V / \partial T)_P / V$) and B_T the isothermal bulk modulus. For the rutile phase of MgF_2 over its entire pressure range, we find that β is approximately proportional to V^t at 300 K, where $t \approx 7$, so giving δ_T a constant value of 7. For the fluorite phase adopted at high pressure [10], in contrast, δ_T decreases with pressure from ≈5.7 at the transition to ≈4.7 at 80 GPa.

3.2 Negative Thermal Expansion – ZrW_2O_8

ZrW_2O_8. exhibits large *negative* thermal expansion [12,13] from 0.3 K to 1050 K; at 428 K there is a transition to a disordered phase, but the ordered phase provides an excellent test of our methods. The unit cell is cubic and comprised of WO_4 tetrahedra sharing corners and ZrO_6 octahedra linked in such a way that each octahedron shares corners with six different WO_4 tetrahedra. Each WO_4 tetrahedron shares only

three of its four oxygens with adjacent ZrO_6 octahedra.

Our QLD calculations for ZrW_2O_8 are analogous to those for MgF_2. For the intra-octahedron O-Zr-O and intra-tetrahedron O-W-O interactions, we used a Urey-energy term $E = \frac{1}{2} k (r_{O-O} - r_e)^2$, where $r_{O\text{-}O}$ is the O-O distance and r_e a constant, rather than an angle term. The calculated linear thermal expansion coefficient α (= β/3) over the range 50 K-300 K is -3.5x10^{-6} K^{-1} (experiment ≈-8.3x10^{-6} K^{-1} [13]).

To understand why this type of cubic structure has negative thermal expansion, we recall the thermodynamic relation $\beta = (\partial S / \partial V)_T / B_T$. Since B_T is always positive, β and $(\partial S/\partial V)_T$ have the same sign. $(\partial S/\partial V)_T$ is negative for ZrW_2O_8 largely due to the Zr-O-W transverse vibrations, which increase in frequency with increasing Zr-W internuclear separation (cf. the transverse vibrations of a stretched violin string). This *tension effect* [14] predominates, in general, only in open structures. A useful and related treatment in terms of "rigid unit modes" has been given by Pryde *et al.* [15].

At pressures over 0.2 GPa, cubic ZrW_2O_8 undergoes a phase transition to a denser orthorhombic phase [16]. In this less open structure, both calculated and observed expansion coefficients are negative and an order of magnitude smaller than for the cubic phase.

3.3 Very low temperatures – polyethylene

At low temperatures C_P and expansion coefficients α_λ are very small, tending to zero as T→0; but they can be measured down to ≈1 K or lower by sensitive techniques [17,18]. Such measurements give information about low energy levels and their strain dependence. At these temperatures MC and MD cannot simulate C_P and α_λ, but the analytical methods of QLD obtain them to high precision if increasingly fine grids are

used for integrating over **q** as **q**=0 is approached [19].

We have applied QLD to short-range models of orthorhombic polyethylene [20]. The unit cell has 3 external and 6 internal degrees of freedom. Zig-zag polymer chains run in the *c*-direction, interacting weakly with neighbouring chains, so that c_{33} is much larger than c_{11} or c_{22}; α_c is therefore small, and negative because of the tension effect in the C-C bonds. Above 100 K, X-ray diffraction shows that α_a and α_b are positive, with α_a about double α_b. At low temperatures dilatometric measurements on drawn samples show that the mean of α_a and α_b remains positive, but do not give separate values. All our models indicate that below about 10 K the anisotropy between α_a and α_b is greatly reduced or even reversed, largely due to a 'rotational tension' effect [14] that rotates bonds in crystals of low symmetry.

3.4 Surface free energies

We have used full minimisation of the free energy to study the {001} and {110} surfaces of MgO, using a well-established set of shell-model potentials [21]. Our strategy differs from the two-region strategy commonly used for static calculations [22,23]. We consider a slab, infinite in two directions and finite in the other. For a thick enough slab the two faces are essentially noninteracting and can be taken as free surfaces.

Fig. 2 shows the calculated temperature dependence of the surface energies. About 10 layers give convergence to 0.001 J m^{-2}, more then twice the number of layers needed for the static energy to converge. Both surface energies decrease with temperature, the {110} rather more markedly. Imaginary frequncies appear at ≈1600 K for the {110} surface, ≈2600 K for the {001} surface, and ≈2900 K for the bulk,

indicating that QLD fails at lower *T* for the surfaces than for the bulk, due possibly to surface modes with large amplitude of vibration. It is tempting to suggest that surface melting occurs at temperatures below the bulk melting temperature (3100 K). Ref. 8 contains results for a wider range of oxide surfaces.

3.5 Defect energies and defect volumes – Ba^{2+} in MgO

A large Ba^{2+} substituted for Mg^{2+} in MgO distorts the lattice greatly. Our detailed study of the defect free energies, enthalpies and volumes over the range 0-1500 K, based on the full minimisation of all strains, has been given previously [24].

A superlattice of defects is introduced throughout the macroscopic crystal. The periodicity is then of the superlattice; the supercell contains many atoms whose equilibrium positions are not wholly determined by symmetry, but are described by a set of dimensionless internal strain coordinates ε_k. Defect properties, denoted by lower case letters (e.g., g_p denotes the change in Gibbs free energy at constant pressure) can then be computed *both* at constant pressure *and* at constant volume; e.g.,

$$f_v = f_v(V,T) = \left\{F_{dc}(V,T) - F_{pc}(V,T)\right\} / N_d \,;\; g_p = g_p(P,T) = \left\{G_{dc}(P,T) - G_{pc}(P,T)\right\} / N_d$$

Subscripts *dc* and *pc* denote 'defect crystal' and 'perfect crystal' respectively, and quantities in capital letters are free energies (*F*,*G*) of the macroscopic crystal; N_d is the total number of defects in the macroscopic crystal. No account therefore is taken here of the configurational entropy of randomly positional defects in the lattice; this is asymptotically correct for a single isolated defect and convergence towards properties of an isolated defect occurs as the superlattice spacing is increased.

To calculate f_v, the external strain is kept constant while the internal degrees of freedom are varied to give the equilibrium configuration at temperature *T*. Similarly, for

g_p, both external and internal strains are varied to be consistent with the specified pressure. u_v and h_p are determined from the terms that contribute to f_v and g_p. The volume of formation of the defect, v_p, follows immediately from the minimisation of $F+P_{ext}V$.

Fig. 3 shows $h_p(T)$ and $u_v(T)$ vs. T, for a supercell of 216 ions containing one Ba^{2+}. h_p is always greater than u_v above $T = 0$; in the *isolated* defect limit [25] $h_p - u_v = (\beta T / \chi_T) v_p$, where v_p is the defect volume. Here both β and v_p are positive. The T-dependence of u_v is much larger than that of h_p and *opposite* in sign. The results confirm the traditional assumption [25,26] that $u_v(0)$ and u_v(static) are fair approximations to $h_p(T)$. u_v(static) is a better approximation when $T > \Theta_D$. While the high temperature values of u_v extrapolate back towards u_v(static), this is not true of h_p. Where, as here, the thermodynamic quantity of interest is determined by the relatively small difference between two large quantities ($h_p \approx 16$ eV, cf. an enthalpy of ≈ 4400 eV for a supercell of 216 ions), the high precision of the lattice dynamics approach is particularly valuable.

3.6 Solid Solutions

Disorder in polar solids has largely been investigated theoretically via point defect calculations (the dilute limit), or, as in the previous section, via supercells. These methods are not readily extended to mixtures or disordered systems with a finite impurity or defect content. Instead, we have developed a configurationally averaged *lattice dynamics* approach to solid solutions [27], which evaluates an appropriate thermodynamic average over a (limited) set of calculations for different configurations of cations within a supercell. If G_k is the optimised free energy of configuration k, the

enthalpy and entropy of the solid solution are approximated by

$$< H >= \frac{\sum_k H_k \exp(-G_k / k_B T)}{\sum_k \exp(-G_k / k_B T)}, \; < S >= \frac{< H >}{T} + k_B \ln \sum_k \exp(-G_k / k_B T)$$

Fig. 4 shows values of ΔH_{mix} for MnO/MgO obtained in this way with a unit cell of 64 atoms and 32 randomly-chosen cation arrangements. The interionic potentials were taken from ref. 28. The cell size and the number of cation arrangements is sufficient to give convergence in ΔH_{mix} to 0.1 kJ mol^{-1}. There is excellent agreement (Fig. 4) between QLD and a novel Monte Carlo exchange (MCX) technique also developed by us for solid solutions [29]. The enthalpy of mixing at 1300 K is symmetric with a maximum ≈5.4 kJ mol^{-1} (50% MgO, 50% MnO). Agreement with the experimental data of Gripenberg *et al.* [30] is good; we do not see the asymmetry reported by Raghavan [31]. The calculated value of ΔH_{mix} varies only slightly with temperature. The failure of the mean field (MF) approximation shows that local structural relaxation or clustering is important.

QLD is particularly useful for quantities such as entropies of mixing since free energies are obtained so readily. ΔS_{mix} includes *both* configurational *and* vibrational contributions; no assumptions are made about the ideality of the solid solution. Thus calculated entropies of mixing for CaO/MgO (for mole fractions of CaO less than 0.15) show that ΔS_{mix} is larger than the "ideal" value; as with the isolated Ba defect in MgO the vibrational contribution is positive. This work is currently being extended to ΔG_{mix} and so to phase diagrams.

4. CONCLUSIONS

QLD is an economical and precise tool not only for the bulk, but also surfaces,

defects and solid solutions. New methods, such as explicit free energy minimisation of a large number of configurations, can deal with high defect levels and increase considerably the contact between experiment and theory in many areas of materials and solid-state research. Future applications include calculating ceramic and minerological data (e.g., phase diagrams), possibly at high pressure, and kinetic and mechanistic aspects of solid state reactions. Codes for ionic solids and metals (using the embedded atom model) are available from the authors.

Many properties are highly sensitive to the interionic potentials. In recent years improved potentials have been obtained by fitting to *ab initio* calculations, but in the long run, with increasing computer power, it may be better to develop direct *ab initio* MD and QLD techniques.

ACKNOWLEDGEMENTS

This work was supported by EPSRC and NERC. GDB acknowledges support from el Consejo Nacional de Investigaciones Científicas y Técnicas de la República Argentina, and his contribution to this work has been possible due to a grant from the Fundación Antorchas.

REFERENCES

1 M.B. Taylor, G.D. Barrera, N.L. Allan, T.H.K. Barron and W.C. Mackrodt, *Comp. Phys. Comm.* **109**: 135 (1998).

2 N.L. Allan, T.H.K. Barron and J.A.O. Bruno, *J. Chem. Phys.* **105**: 8300 (1996).

3 L.N. Kantorovich, *Phys. Rev. B* **51**: 3520, 3535 (1995).

4 A.B. Pippard, *The Elements of Classical Thermodynamics,* (Cambridge University Press, Cambridge, 1964).

5 D.C. Wallace, *Thermodynamics of Crystals* (Wiley, New York, 1972).

6 M.B. Taylor, G.D. Barrera, N.L. Allan and T.H.K. Barron, *Phys. Rev. B* **57**: 14380 (1997).

7 M.B. Taylor, N.L. Allan, J.A.O. Bruno and G.D. Barrera, *Phys. Rev. B* **59**: 353 (1999).

8 M.B. Taylor, C.E. Sims, G.D. Barrera and N.L. Allan, *Phys. Rev. B* **59**: 6742 (1999).

9 P.J. Harley in *Numerical Algorithms,* J.L. Mohamed and J.E. Walsh, ed. (Clarendon Press, Oxford, 1986), p. 239.

10 G.D. Barrera, M.B. Taylor, N.L. Allan, T.H.K. Barron, L.N. Kantorovich and W.C. Mackrodt, *J. Chem. Phys.* **107**: 4337 (1997).

11 Y.S. Touloukian, R.K. Kirby, R.E. Taylor and T.Y.R. Lee, eds., *Thermophysical props. of matter (TPRC Data Series),* vol. 13, (IFI/Plenum, New York-Washington, 1977).

12 T.A. Mary, J.S.O. Evans, T. Vogt and A.W. Sleight, *Science,* **272**: 90 (1996).

13 J.S.O. Evans, T.A. Mary, T. Vogt, M.A. Subramanian and A.W. Sleight, *Chem. Mater.* **8**: 2809 (1996).

14 T.H.K. Barron, in *Thermal Expansion of Solids,* C.Y. Ho, ed. (ASM International, Materials Park, Ohio, 1998), pp. 1-108.

15 A.K.A. Pryde, K.D. Hammonds, M.T. Dove, V. Heine, J.D. Gale and M.C. Warren, *J. Phys. Condens. Matter* **8**: 10973 (1996).

16 J.S.O. Evans, Z. Hu, J.D. Jorgensen, D.N. Argyriou, S. Short and A.W. Sleight, *Science*, **275**: 61 (1997).

17 C.A. Svenson, in *Thermal Expansion of Solids*, C.Y. Ho, ed. (ASM International, Materials Park, Ohio, 1998), pp. 207-224.

18 T.H.K. Barron and G.K. White, *Heat Capacity and Thermal Expansion at Low Temperatures* (Kluwer Academic/ Plenum, New York, 1999).

19 J.A.O. Bruno, N.L. Allan and T.H.K. Barron, *J. Phys. Condens. Matter* **12**: 549 (2000)

20 J.A.O. Bruno, N.L. Allan, T.H.K. Barron and A.D. Turner, *Phys. Rev. B* **58**: 8416 (1998).

21 A.M. Stoneham and M.J.L. Sangster, *Phil. Mag. B* **43**: 597 (1981).

22 P.W. Tasker in *Computer Simulation of Solids*, C.R.A. Catlow and W.C. Mackrodt, eds. (Springer-Verlag, Berlin, 1982), p. 288.

23 E.g., D.H. Gay and A.L. Rohl, *J. Chem. Soc., Faraday Trans*. **91**: 925 (1995).

24 M.B. Taylor, G.D. Barrera, N.L Allan, T.H.K. Barron and W.C. Mackrodt, *Farad. Discuss.* **106**: 377 (1997).

25 C.R.A. Catlow, J. Corish, P.W.M. Jacobs and A.B. Lidiard, *J. Phys. C* **14**: L125 (1981).

26 N.L. Allan. W.C. Mackrodt and M. Leslie, *Adv. Ceram.*, **23**: 257 (1987).

27 J.A. Purton, J.D. Blundy, M.B. Taylor, G.D. Barrera and N.L. Allan, *Chem. Commun.* 627 (1998).

28 G.V. Lewis and C.R.A. Catlow, *J. Phys. Sol. State Phys.* **18**: 1149 (1985).

29 J.A. Purton, G.D. Barrera, N.L. Allan and J.D. Blundy, *J. Phys. Chem. B* **102**: 5202 (1998).

30 S. Raghavan, Ph.D. Thesis, Indian Institute of Science, Bangalore, India, 1971.

31 H. Gripenberg, S. Seetharaman and L.I. Staffansson, *Chem. Scr.* **13**: 162 (1978-9).

FIGURE CAPTIONS

Fig. 1

Calculated values of a and c for MgF_2, with experimental data from ref. 11.

Fig. 2

Calculated surface energies for MgO.

Fig. 3

Temperature variation of h_p (◊) and u_v (+) for a supercell containing 216 ions. $u_v(0)$ and u_v(static) are also shown.

Fig. 4

Calculated values of ΔH_{mix} at 1000 K for MnO/MgO given by configurational lattice dynamics (QLD), exchange Monte Carlo (MCX) and mean field theory (MF). Two sets of experimental data are also shown (RG from ref. 30, GP from ref. 31).

Fig. 1

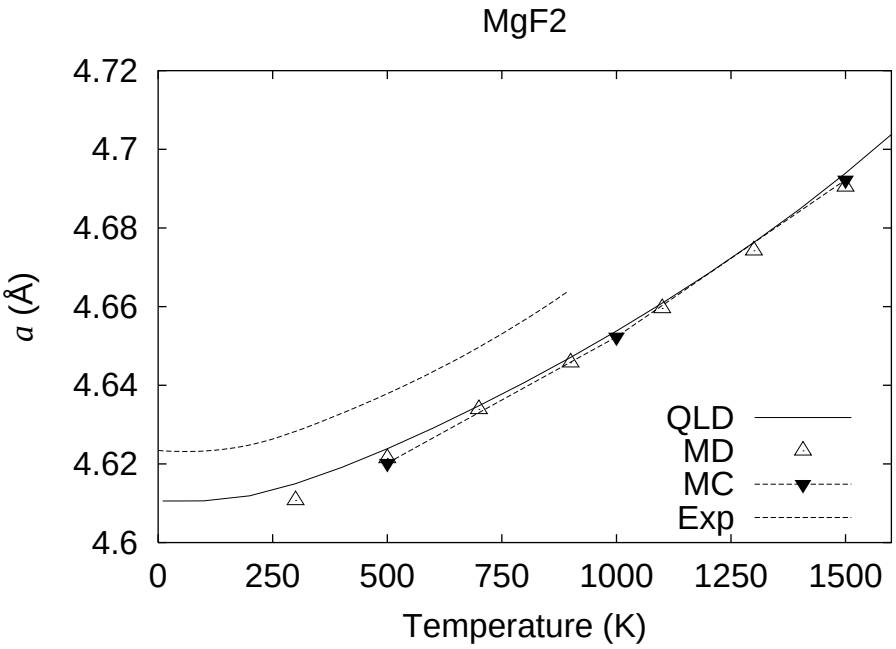
MgF2
4.72
4.7
4.68
4.66
4.64
4.62
4.6
a (Å)
0
250
500
750
1000
1250
1500
Temperature (K)
QLD
MD
MC
Exp

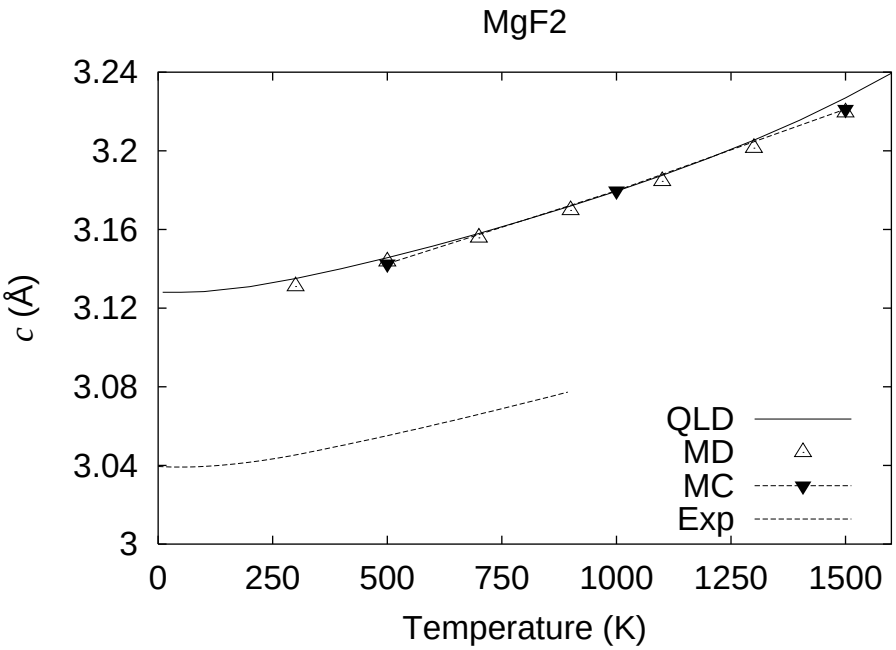
MgF2
3.24
3.2
3.16
3.12
3.08
3.04
3
c (Å)
0
250
500
750
1000
1250
1500
Temperature (K)
QLD
MD
MC
Exp

Fig. 2

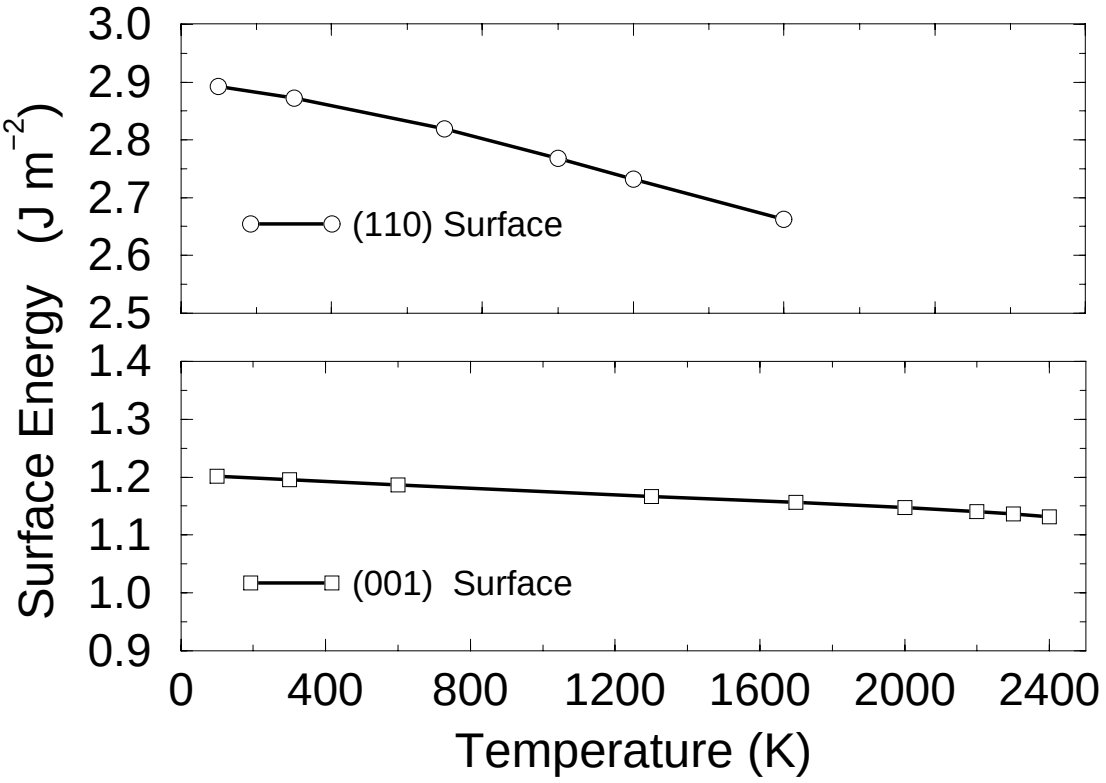
3.0
2.9
2.8
2.7
2.6
2.5
1.4
1.3
1.2
1.1
1.0
0.9
Surface Energy (J m^{-2})
(110) Surface
(001) Surface
0
400
800
1200
1600
2000
2400
Temperature (K)

Fig. 3

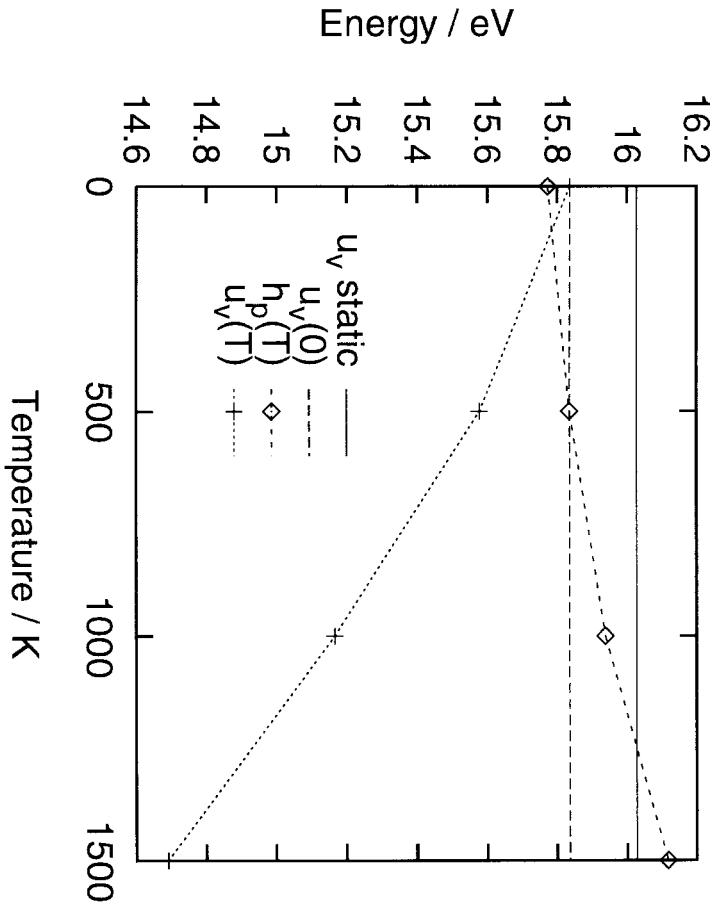
Energy / eV
16.2
16
15.8
15.6
15.4
15.2
15
14.8
14.6
0
500
1000
1500
Temperature / K
u_V static
$u_V(0)$
$h_p(T)$
$u_V(T)$

Fig. 4

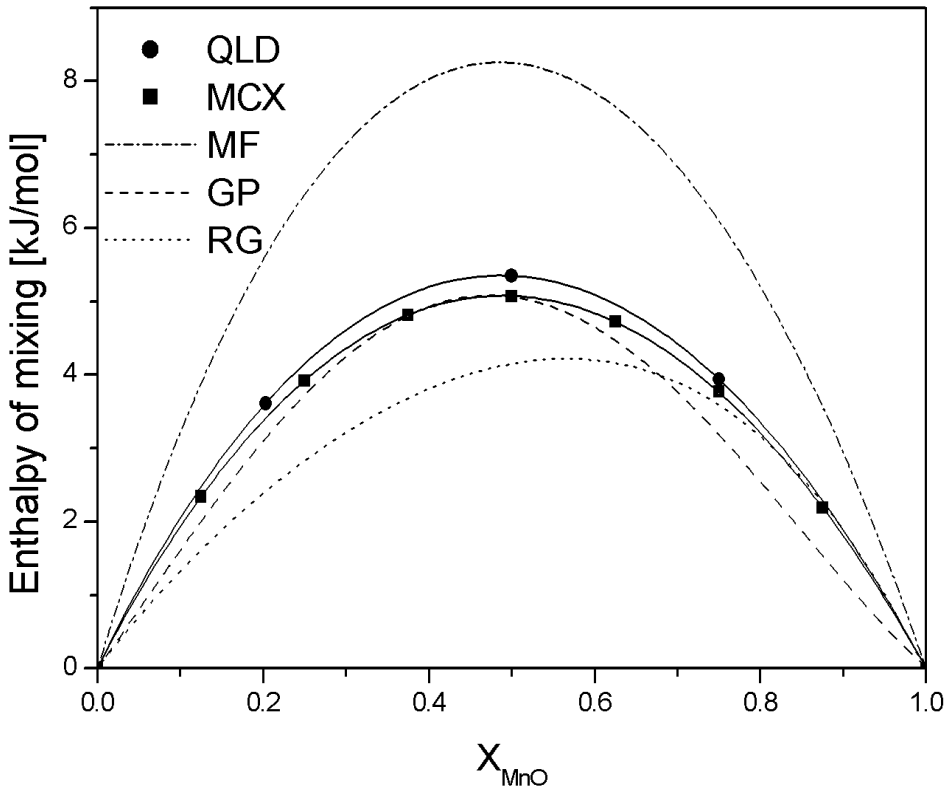
QLD
MCX
MF
GP
RG
Enthalpy of mixing [kJ/mol]
0
2
4
6
8
0.0
0.2
0.4
0.6
0.8
1.0
X_MnO